Journal of Materials Chemistry A

COMMUNICATION

View Article Online
View Journal | View Issue

Cite this: J. Mater. Chem. A, 2017, 5, 4300

Received 4th January 2017
Accepted 24th January 2017

DOI: 10.1039/c7ta00069c

rsc.li/materials-a

A soft non-porous separator and its effectiveness in stabilizing Li metal anodes cycling at 10 mA cm^{-2} observed *in situ* in a capillary cell†

Kai Liu,[ab] Peng Bai,[c] Martin Z. Bazant,[cd] Chang-An Wang*[a] and Ju Li*[be]

While lithium metal anodes have the highest theoretical capacity for rechargeable batteries, they are plagued by the growth of lithium dendrites, side reactions, and a moving contact interface with the electrolyte during cycling. Here, we synthesize a non-porous, elastomeric solid–electrolyte separator, which not only blocks dendritic growth more effectively than traditional polyolefin separators at large current densities, but also accommodates the large volume change of lithium metal by elastic deformation and conformal interfacial motion. Specially designed transparent capillary cells were assembled to observe the dynamics of the lithium/rubber interface *in situ*. Further experiments in coin cells at a current density of 10 mA cm^{-2} and an areal capacity of 10 mA h cm^{-2} show improved cycling stability with this new rubber separator.

Lithium metal anodes, which have extremely high capacity and low redox potential, are key for next-generation batteries.[1,2] However, they suffers from a poor safety reputation, low coulombic efficiency, and short cycle life,[3,4] where uneven growth of lithium[5] is believed to be the root cause. Non-uniform electrodeposition roughens the lithium/electrolyte interface and increases the lithium anode surface area, onto which a new solid–electrolyte interphase (SEI) layer forms; this SEI growth associated with interfacial roughening during cycling is not reversible, which continually consumes active lithium and the electrolyte, yielding a very low coulombic efficiency and short cycle life.[4,6,7] Meanwhile, during discharge, the root of a lithium metal protrusion is often dissolved first, making the top part disconnected, causing electronically isolated lithium (dead lithium)[8,9] and therefore capacity loss. Moreover, lithium may grow through the pores of traditional porous separators to short-circuit the cell internally, which may lead to thermal runaway and even explosion.

Solid electrolytes, such as solid ceramic,[10–13] polymer[14,15] or composite[16–18] materials, can function as a separator and electrolyte at the same time. Take a fully dense ceramic as an example; its non-porous structures and high strength can help stop lithium dendrite penetration and enhance the safety of lithium metal batteries. However, the ionic conductivity of ceramic electrolytes is often not high enough, and the large dimensional change of lithium metal during cycling makes it difficult to maintain good contact inside the battery.[19] The lithium metal necessarily needs to retract during discharging, and maintaining good contact of a moving interface with a solid electrolyte over a long distance for Li^+ conduction is quite challenging, especially if the lithium morphology has already roughened or even turned porous.

When swollen with a liquid electrolyte, a soft elastic and fully dense (non-porous) solid–electrolyte separator may have a high ionic conductivity, and at the same time improve the contact quality, like a blown-up balloon with self-stress that can help store and eject gas reversibly. Fig. 1b shows a schematic design. Compared to traditional porous separators, with a limited ability to accommodate uneven volume change and in which ~30 nm open pores concentrate the current to induce heterogeneous diffusion-limited growth and penetration,[20] a fully dense and uniform elastomeric solid–electrolyte separator has no risk of "chasing the current" through open pores. When a separator can deform elastically, it also automatically exerts a compressive stress against lithium anodes when resisting local volume expansion to keep uniform interfacial contact and limit the deterioration of the lithium morphology. A widely accepted guideline in the battery literature is that the shear modulus of a Li-ion-conducting electrode separator should

[a]State Key Lab of New Ceramics and Fine Processing, School of Materials Science and Engineering, Tsinghua University, Beijing 100084, P. R. China. E-mail: wangca@mail.tsinghua.edu.cn

[b]Department of Nuclear Science and Engineering, Massachusetts Institute of Technology, Cambridge, Massachusetts 02139, USA. E-mail: liju@mit.edu

[c]Department of Chemical Engineering, Massachusetts Institute of Technology, Cambridge, Massachusetts 02139, USA

[d]Department of Mathematics, Massachusetts Institute of Technology, Cambridge, Massachusetts 02139, USA

[e]Department of Materials Science and Engineering, Massachusetts Institute of Technology, Cambridge, Massachusetts 02139, USA

† Electronic supplementary information (ESI) available. See DOI: 10.1039/c7ta00069c

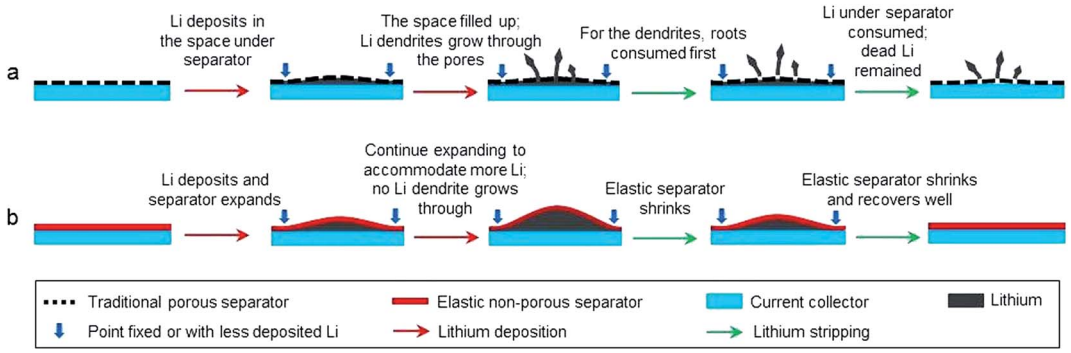

Fig. 1 Schematics of the behaviors of a traditional plastic porous separator (a) and a designed non-porous elastomeric solid–electrolyte separator (b) interacting with uneven lithium deposition at high current densities and large areal capacities.

exceed 6.8 GPa in order to block dendrite penetration.[21] In contrast, here we report a non-porous soft rubber separator with a large elastic deformation range and show that even if the separator is softer by a factor of 10^4, dendrite penetration can still be prevented. Our rubber separator, which is distinct from a common polymer electrolyte/separator in terms of the supramolecular structure, mechanical properties, matrix porosity and preparation method, has a high ionic conductivity and unexpectedly high lithium ion transference number (t_+), and performs well in coin cells at a high current density of 10 mA cm^{-2} and capacity of 10 mA h cm^{-2}. These results reveal that an elastomeric solid–electrolyte separator can vastly improve the performance of a lithium metal anode.

The rubbery material, in which molecules associate together to form chains and cross-links *via* hydrogen bonds, was synthesized by reaction of fatty acids, diethylenetriamine and urea (Fig. S1–S3†), and hot pressed to form a non-porous membrane. As shown in Fig. 2a–c, before the immersion in an organic liquid electrolyte, the diameter and thickness of the rubber separator were ~16 mm and ~90 μm, respectively, and the separator has no visible pores at the highest magnification of the scanning electron microscope (SEM). For comparison, there are extensive pores with a mean diameter around 30 nm in traditional PP separators (Celgard 2400, Fig. S5†). After a 30 day immersion in an organic liquid electrolyte, the diameter increased to ~19 mm, and the thickness increased to ~100 μm (Fig. 2d and f). There were still no pores in the separator and no obvious dissolution of the material (Fig. 2e). These results indicate that the rubber can accommodate limited swelling in the liquid bath to form a single-phase solid–electrolyte alloy with the salt/solvent at the molecular scale, which is similar to hydrated Nafion. Therefore, the Li^+ conduction mechanism could also change from vehicular motion of a large solvation shell structure to the kick-out ion exchange ("Grotthuss") mechanism.[22,23] As shown in Fig. 3a, during immersion, the weight gain of the rubber separator increased with the soaking time in the first 4 hours and then leveled off at ~125 wt% gain. TG-FTIR tests reveal that the liquid electrolyte imbibed into the

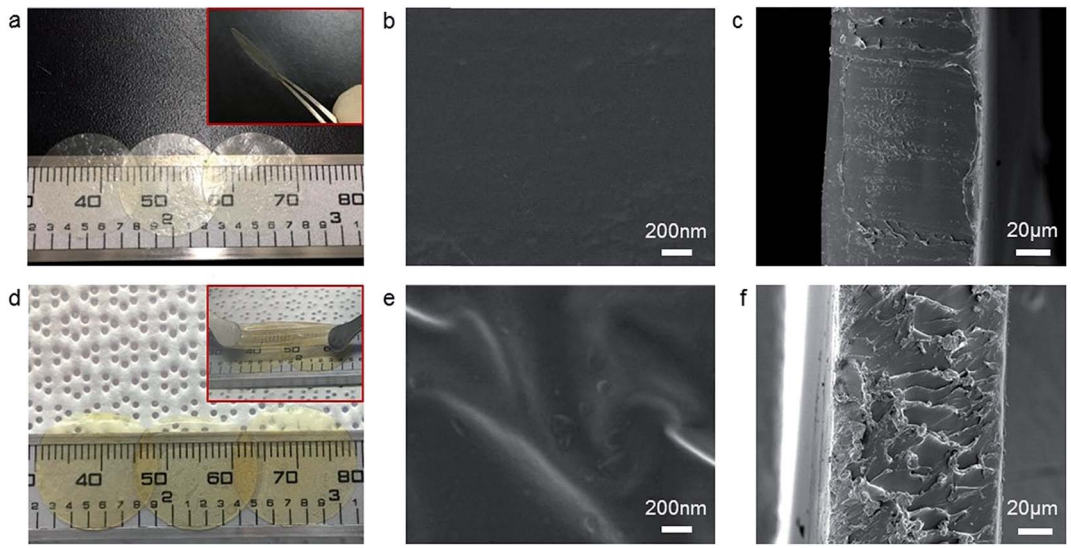

Fig. 2 Digital photos, SEM images of the surfaces and cross sections of the rubber separators before (a–c) and after (d–f) swelling in the organic liquid electrolyte for 30 days.

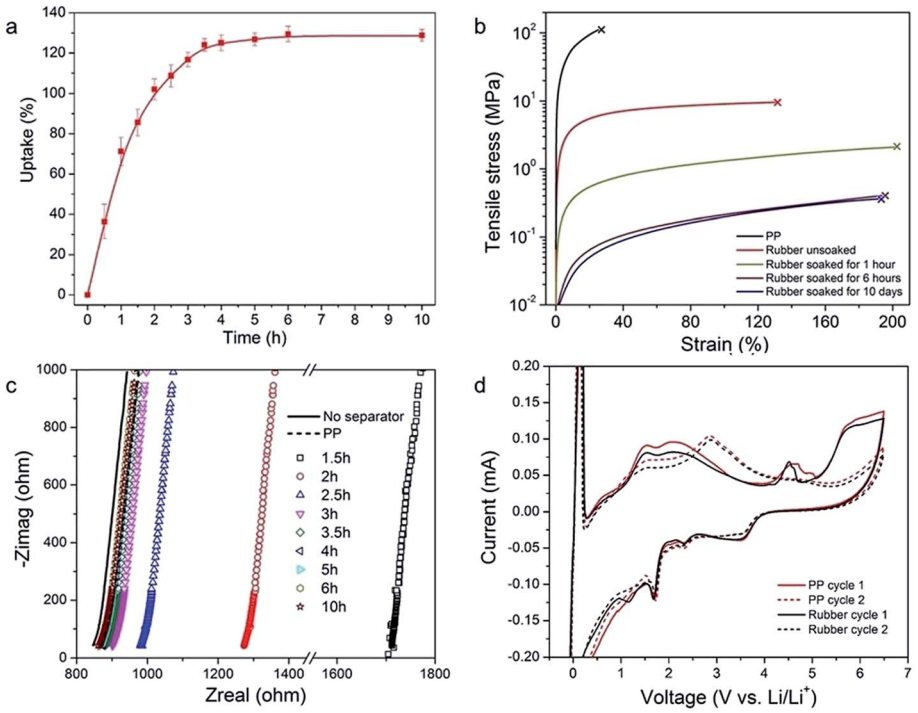

Fig. 3 Effects of organic liquid electrolyte uptake on the mechanical and electrochemical properties of the rubber separator. (a) Organic liquid electrolyte uptake by the rubber separator. (b) Tensile test results of the rubber separator samples after different soaking times, with a PP separator as the control. Loading rate: 0.5 N min^{-1}. (c) AC impedance spectra of the H-cell with rubber separators measured within 1.5–10 h after the assembly, where those of the porous PP separator and pure electrolyte (no separator) are also given for comparison. (d) CV curves of Li-stainless steel coin cells. Scan from −0.2 to 6.5 V at a scan rate of 5 mV s^{-1}.

rubber separator has the same solvent composition (EC : EMC = 3 : 7 by volume) as the bulk liquid electrolyte, but has a higher $LiPF_6$ salt uptake (Fig. S6 and S7†). Fig. 3b shows that the tensile strength of the rubber, ~10 MPa, is much lower than that of the Celgard PP separator (~110 MPa) and further decreases to ~0.4 MPa after being saturated with an organic liquid electrolyte. However, the tensile failure strain of the swelled rubber (~200%) is much higher than that of PP, and a fully reversible strain recovery can be seen after a tensile deformation up to a strain of 100% (Video S1†).

To monitor the evolution of Li-ion conducting capability while soaking, an organic liquid electrolyte filled H-type cell with two Pt electrodes and a rubber separator in between was assembled (Fig. S8†). For comparison, H-type cells employing no separator, the porous PP separator, and a dense PVDF separator without any ionic conductivity were also assembled and tested. AC impedance spectra of the H-type cells are given in Fig. 3c. In the first 1 hour after assembly, the impedance spectrum of the rubber separator consisted of random spots, as observed in the control case of the PVDF separator (Fig. S9†), indicating that the lithium ion conductive pathways had not yet been established. However, after immersion for 1.5 hours, with the liquid electrolyte uptake into the solid rubber exceeding 80 wt%, the impedance spectrum assumed the shape of a diagonal line, roughly parallel to the spectra of the cells using no separator and the PP separator, but shifted to a much higher resistance (real part of the impedance). With increasing soak time, this additional resistance dropped in proportion to the liquid uptake and reached the same low value as that of the PP separator based H cell. Both the impedance arcs of the cells employing the PP and rubber separators slightly shifted from that of the separator-free cell. This shift (~20 Ω) is counted as the resistance caused by the separators. Sandwich structured stainless-steel/separator/stainless-steel cell tests also showed the swollen rubber separator's good ionic conductivity (Fig. S10†). Interestingly, the swollen rubber separator also has a high t_+ of 0.76 (Fig. S11†). The high t_+ may be attributed to the "Grotthuss" mechanism of Li^+ transport in confined spaces that replaces vehicular transport of the full solvation shell structures of both anions and cations. Also, hydrogen bonds between the weakly acidic protons (protons connected to amidic N) in the rubber molecule and the F atoms in $[PF_6]^-$ anions may restrict the movement of the anions, which in typical liquid electrolytes diffuse faster than Li^+ cations. These results confirmed the rubber separator's excellent capability to conduct lithium ions after adequate alloying. A ~125 wt% weight gain means the "solid network" and the "fluid penetrant" have about equal proportions in the alloy, and thus can be both globally percolating: if like Nafion the Li^+ hops along the "fluid penetrant" molecular chains, then the areal density of such conducting chains could be very high, and Li^+ conduction would still appear highly uniform seen at the smallest capillary-size scale of mossy lithium, which is tens of nanometers,[8] unlike the PP separator with conduction heterogeneity at the tens of nanometers scale. The CV curves of the coin cells using our rubber separator and the PP separator are highly similar, see Fig. 3d, indicating that

the rubber separator did not cause extra side reactions in cycling. A long-term interfacial stability between lithium and the rubber separator is also observed (Fig. S12†). These results confirm that the weakly acidic protons do not affect the compatibility of the rubber separator with lithium.

To verify the separator's ability to accommodate lithium electrode volume change and conform to the moving lithium morphology, transparent glass capillary cells,[5] containing either a PP or a rubber membrane or no membrane, were fabricated to study the interactions *in situ*. The structure of the capillary cells is shown in Fig. S13.† Six discharge–charge cycles of the capillary cells at a constant current density of 10 mA cm^{-2} (with respect to the exposed area (unpainted) of a copper wire electrode) were conducted, and the dynamics of the electrode interface were videotaped. In each cycle, we first discharge for a certain period of time to deposit lithium onto the bare section (no red paint) of the copper wire, and then charge to strip the lithium until the voltage rises to 5 V.

Fig. 4a shows the cycling behavior of the capillary cell without any separator. In the first 240 seconds, lithium metal deposited relatively uniformly, while from the 240th second onwards, as pointed out by the white arrow, clusters of porous lithium deposits began to grow, and resulted in a layer of mossy lithium on the top at the end of discharge. In the following charge process, the deposited lithium shrunk while its color became darker and darker, which indicated the reaction between lithium metal and the organic liquid electrolyte and the development of porosity. At the 420th second of charge, a layer of dark grey product remained and could not be stripped, which should be dead lithium and a SEI on its surface. Meanwhile, the charge voltage rose sharply (Fig. 5a), and small bubbles were generated, which merged and grew bigger in the following cycles. However, the bubbles evolved only once, toward the end of the first charge with high voltage, despite the fact that the voltage rose equally high in the following charge cycles. This must be due to SEI passivation on the surface of the copper wire electrode. As shown in Fig. 5a, the charge–discharge voltage gap increased with the cycle number, which indicated the increase of the internal resistance. After six cycles, a thick layer of dark grey product, which could not be cycled anymore, accumulated on the working electrode. The growth of this product is the likely cause of the dramatically decreased coulombic efficiency, as shown in Fig. 6d. It can be concluded that, without any mechanical restriction, lithium metal electrodes grow non-uniformly to form highly porous structures with a large specific surface area very quickly upon cycling.

Fig. 4b shows the interaction between the porous PP separator and the lithium metal electrode. During discharge, lithium metal deposited onto the copper wire electrode under the PP separator. However, at the 405th second, a lithium dendrite penetrated through the PP separator and continued growing above it, as indicated by the upper red arrow. In a coin cell, such lithium dendrite breaking through leads to internal short circuits (Fig. S14†). Meanwhile, as labeled by the lower red arrow, some lithium grew through the gap between the enameled copper wire and PP separator due to incomplete encapsulation by the separator. At the end of the first discharge, there were several lithium dendrites deposited above the separator, which could not be stripped while charging and eventually became "dead lithium". During the entire test, the PP separator barely deformed, indicating that the mechanical stress exerted by growing lithium whiskers and dendrites was insufficient to

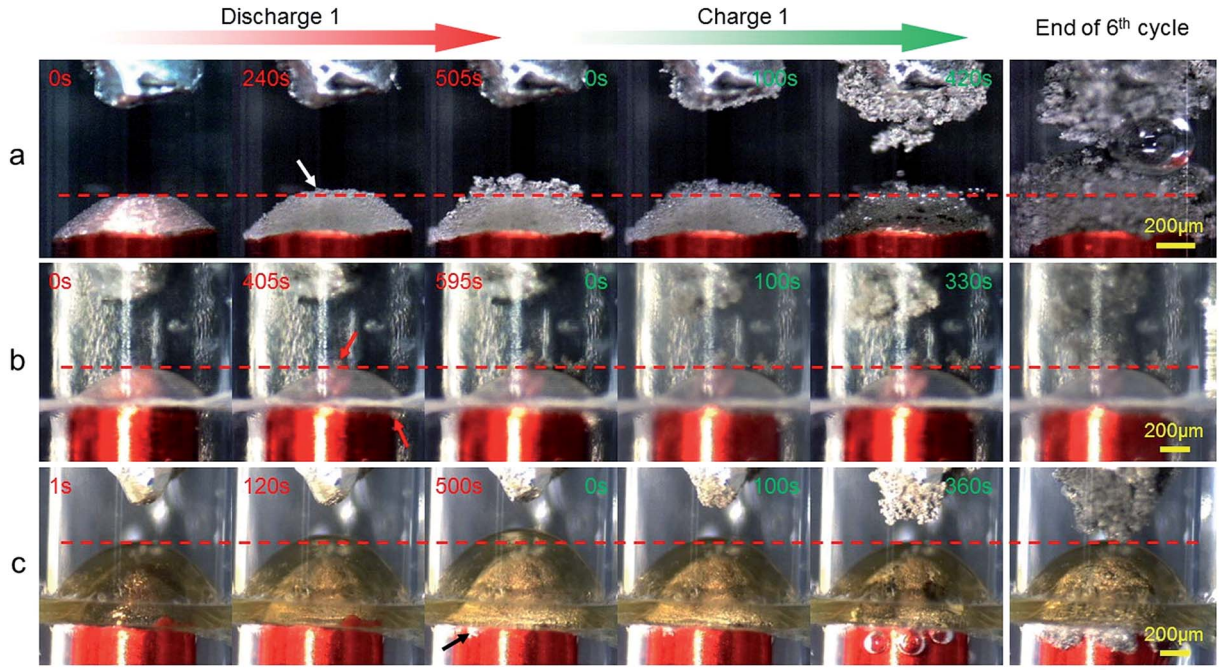

Fig. 4 *In situ* snapshots of the capillary cells during the first cycle and at the end of the last cycle, (a) without any separator (Video S2†), (b) with a PP separator (Video S3†), and (c) with our rubber separator (Video S5†).

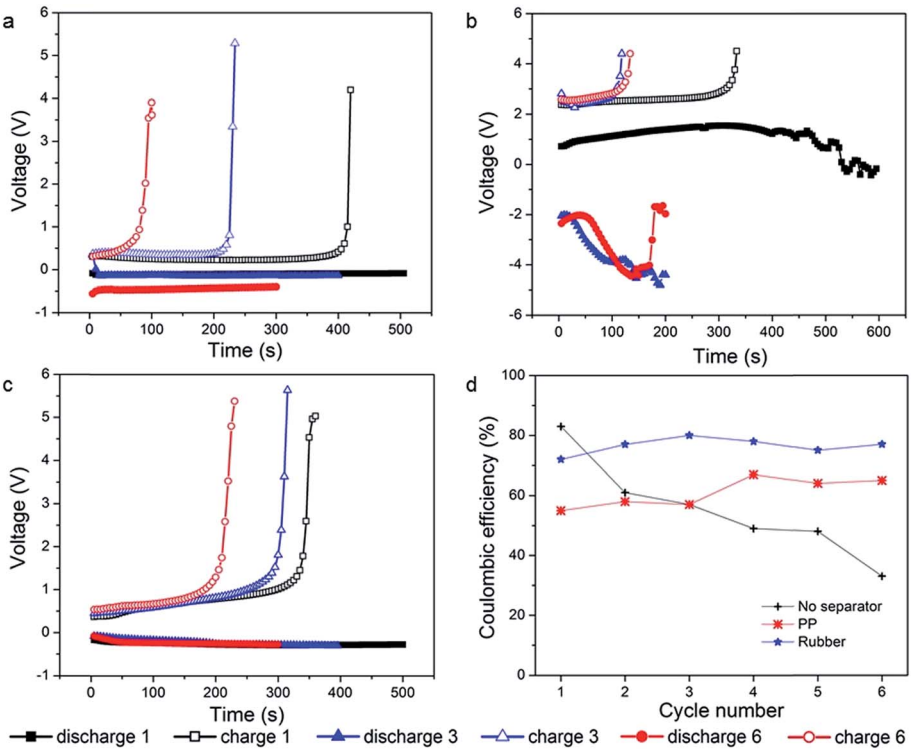

Fig. 5 Cycling performance of the capillary cells. 1st, 3rd, and 6th discharge–charge curves of the capillary cells (a) without a separator, (b) with a porous PP separator and (c) with the rubber separator; (d) coulombic efficiency of the corresponding capillary cells.

deform the PP separator. The PP separator was removed and cleaned in ethanol after the cycling and observed using a SEM. No breakage was found, and the porous structure of the separator was well maintained (Fig. S15†). Therefore, it is reasonable to infer that it was along the original pores of the PP separator that the lithium dendrites grew and finally penetrated through. It can be imagined that when confined within the pores of the separator, the lithium dendrites should be very thin, sparse and fragile, possibly plating along the internal pore surfaces at high rates, as observed for copper electrodeposition in nanoporous media.[24,25] During charging, the thin parts of the dendrites inside the separator were consumed first and quickly, and therefore the outer part of the dendrites loses electrical contact with the electrode and becomes "dead lithium". Fig. 5b shows typical discharge–charge curves of the cycles. In the first discharge, the discharge voltage suffered a fluctuation after lithium dendrites grow through the separator. In the subsequent cycles, the charge–discharge voltage gap became much larger, indicating a huge increase in the internal resistance. Referring to the behavior of the cell without a separator, this phenomenon could be attributed to the blockage between the electrode and the separator caused by a sheet of gas bubbles (akin to the Leidenfrost effect), which were generated at the end of the first charge when the local voltage became too low (relative voltage too high). After the sixth charge, there were some lithium dendrites and a layer of grey reaction products observable above and beneath the PP separator, respectively. However, the total amount of lithium, per volume or per area, was much less than that in the cell without a separator. The coulombic efficiency of the cell remained stable at ~60% and did not drop with increasing cycle number (Fig. 5d). This could be attributed to a small increase in the surface area of lithium metal due to SEI formation on the working electrode, constrained by the PP separator. Nevertheless, the formation of the "dead lithium" still contributes to the loss of the active material in each cycle. Another capillary cell was assembled using the same PP separator, and cycled at a current density of 100 mA cm^{-2}, where the process of dendrite penetration leading to "dead lithium" can be seen more clearly (Video S4†).

Fig. 4c shows the behavior of the lithium metal electrode covered by our elastomeric separator. It is clear that the separator expanded as lithium metal deposited onto the copper wire electrode beneath it, and the deposited lithium had a relatively flat morphology without any large-sized lithium protrusions that could begin to puncture the separator. Because of the non-porous structure of the rubber separator, there was no easy access for lithium dendrites to grow through. Stable cycling of a coin cell with the rubber separator fixed by an O-type washer confirmed the suppression of lithium dendrite penetration on a larger scale (Fig. S14†). As in the PP based cell, some leakage of deposited lithium can also be found in the gap between the enameled copper wire and the glass capillary due to the incomplete encapsulation by the rubber, as indicated by the black arrow. While charging, with stripping of lithium metal, the expanded elastomeric separator shrunk back gradually to its original position. Just like a balloon, the rubber separator can expand and shrink repeatedly following the volume change of the lithium metal electrode. At the end of the first charge, gas

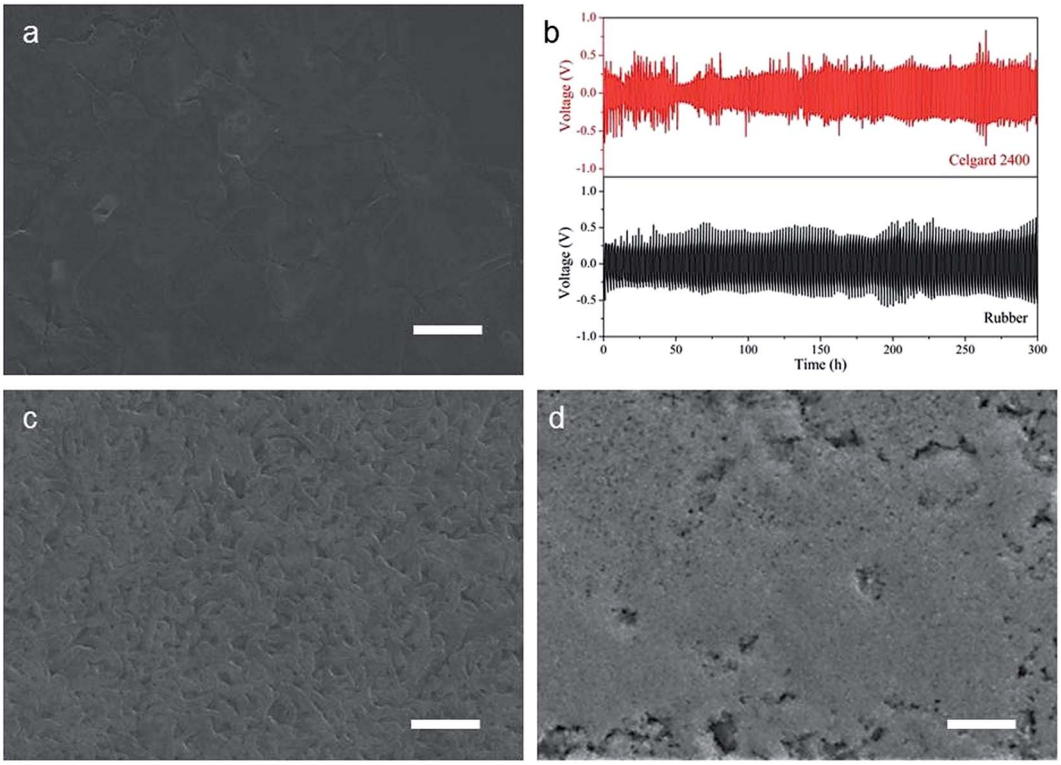

Fig. 6 Typical scanning electron microscopy images of metallic lithium anodes and charge–discharge curves. (a) Surface of fresh lithium metal. (b) Cycling profile of Li–Li symmetrical coin cells at a current density of 10 mA cm^{-2} and areal capacity of 10 mA h cm^{-2}. (c) Surface of the lithium metal electrode of the cell using Celgard 2400 after 150 cycles. (d) Surface of the lithium metal electrode of the cell using the rubber separator after 150 cycles. The white scale bar represents 5 μm for all the images.

bubbles were generated as well, but interestingly, instead of gathering into a blocking sheet between the electrode and separator, most, if not all, of the gas bubbles were expelled by the stressed rubber separator. As a result, gas bubbles did not affect the quality of electrical contact in the following cycles. After six cycles, there was also a layer of grey matter left on the copper wire electrode, but the layer was less rough. The improvement of the lithium electrode morphology could be attributed to the uniform pressure created by the elastic rubber separator in response to the volume expansion of the lithium anode, and the high t_+, which is well known to help reduce the dendritic instability tendency.[26,27] These two features of the rubber separator enable its high reliability.

From Fig. 5c we can see that, discharge–charge curves of the capillary cell employing the rubber separator were very stable. There was almost no change in the charge–discharge voltage gap, which indicated a stable internal resistance and a good moving electrode–electrolyte contact, in spite of the existence of side reactions and bubbles. Although the coulombic efficiency of the rubber separator based cell was not high (Fig. 5d), which may be due to the side leakage of the deposited lithium through incomplete encapsulation, it was still the highest and the most stable result among the three kinds of capillary cells. All of these results confirm that the rubber separator enhanced the cycling performance and rate capability of the lithium metal anode.

Since the ~0.4 MPa modulus of our rubber is exceedingly small compared to those of hard materials, it is intriguing why it is still effective in improving the performance of the lithium metal anode. We believe that ~0.4 MPa matches with ("resonates with") the effective modulus of mossy lithium, a highly porous solid. Dense lithium metal has a shear modulus of 3.4 GPa; according to the modulus-density scaling for highly porous fractals,[28] $E/E_s \sim (\rho/\rho_s)^{3.6}$, so 90% porous mossy lithium gives rise to a MPa level modulus. Thus, as we have seen, the growth and shrinkage of mossy lithium can actuate the rubber separator, and the resulting resisting pressure from the rubber and the long range of elasticity is also large enough to influence the mossy lithium morphology and improve the contact quality, as their moduli and ranges of motion are "in resonance". The stable discharge–charge curves and relatively high coulombic efficiency of the capillary cell establish the effectiveness of such a mechanically soft but Li^+ conduction-wise uniform barrier. Let us consider two limiting scenarios where the electrolyte modulus is "off-resonance" with that of mossy lithium: one being too hard (as in dense ceramics), and the other being too soft (as in liquid electrolytes, with zero modulus). The former scenario tends to have a contact problem with the moving interface, since the electrolyte cannot conform and adjust to retreating lithium – indeed it is difficult to imagine a dense ceramic electrolyte adjusting itself to the inevitable configurational perturbations in manufacturing and cycling, and keep engulfing potentially roughening/plastically deforming/porous lithium. Liquid electrolytes do not have this contact quality problem, and they can adjust to any changing conformation

very easily, but their zero modulus does not limit porous lithium or impede dendrite growth mechanically at all, so the lithium morphology becomes increasingly porous and highly non-uniform in just a few cycles. The number of side reactions increases in each cycle due to the increasing surface area of the lithium metal, leading to a dramatically decreasing coulombic efficiency. The PP membrane, which combines "too soft" open pores and "too hard" polymers, has an additional disadvantage of heterogeneous Li^+ conduction, which induces morphological instability in cycling. Once the lithium has no space to grow under the PP separator, the rigid confinement of the "too hard" polymer and the heterogeneous conduction ("chasing after current") will force it to grow inside the pores of the separator, eventually leading to penetration. The contact impedance also grows dramatically. The results of the visual capillary cell experiments confirm the hypothesis illustrated in Fig. 1.

To further investigate the effectiveness of the rubber separator, symmetrical Li–Li coin cells (same as the structure of the coin cell in Fig. S14† but without the O-type washer) were assembled using the swollen rubber separator, as well as the porous PP separator control, and cycled at 10 mA cm^{-2} with a high discharge–charge capacity of 10 mA h cm^{-2}. As shown in Fig. 6c, after 150 cycles of the Celgard 2400 based cell, the lithium's surface layer became compacted with micron and sub-micron sized dendrites. Most of the dendrites were blocked and planarized by the PP separator. However, as can be seen in Fig. 6b, there was an obvious voltage drop at the $\sim 50^{th}$ hour, which indicating an internal short. This should correspond to current-chasing dendrites growing through the separator, just like the situation of the capillary cell. For the rubber separator based cell, no sudden voltage drop was observed, indicating no penetration.

In summary, we have provided a new strategy to enhance the performance of a lithium metal anode by using non-porous elastomeric solid electrolytes as separators. Our *in situ* observation of capillary cells demonstrates its advantages over traditional porous PP separators in terms of suppressing lithium dendrite growth and accommodating the large volume change of a lithium metal anode, especially at a high current density with a high discharge–charge capacity. Considering the diversity of rubber materials, it should be possible to find or develop still better non-porous rubbery solid electrolyte separators with a larger reversible elastic strain range, high electrochemical and chemical stabilities, "resonating" modulus but high mechanical strength and low cost, to help enable practical batteries with lithium metal anodes.

Experimental

Synthesis of the rubber separator

The elastomeric separator we used in this work was synthesized following the procedure reported by L. Leibler *et al.*[29] (Fig. S1†). Specifically, 175 g of Empol 1016 fatty dimer acid (mixture of 4% monoacid, 79% diacid, 17% triacid and polyacids, supplied by Cognis) was condensed with 70.3 g of diethylenetriamine (Alfa, 99%) at 160 °C under nitrogen protection over 24 h. After eliminating unreacted amine by the chloroform/water extraction method, oligo-amidoamine was obtained. Then, 72 g of the oligo-amidoamine was mixed with 17 g urea (Alfa, 99.3+%). The mixture was heated under nitrogen protection at 135 °C for 1.5 h, and then the temperature was increased up to 160 °C by 5 °C increments every 60 min. After reaction, ammonia and unreacted urea were extracted by vacuum stripping and water washings. The obtained material was dried under vacuum and hot pressed at 120 °C into membranes with a thickness of ~90 μm. Finally, the membrane is immersed in an organic liquid electrolyte (1 M $LiPF_6$ in EC/EMC (3 : 7 v/v) purchased from Ube Industries, Japan) to swell. The reaction process was monitored using FTIR and ^1H NMR (Fig. S2 and S3†).

Characterization of the rubber separator

For AC impedance measurements, the two gaskets made of silicone rubber in the H-type cell are clamped very tightly to ensure that there is no leakage and no liquid electrolyte crossover. The AC impedance was measured using a Gamry Reference 3000 workstation with a frequency range of 1 Hz to 1 MHz and an amplitude of 5 mV at room temperature.

The electrolyte uptake in the rubber separators (5 samples in total) with swelling was determined by measuring the weight increase and calculated according to the equation below:

$$\text{Uptake } (\%) = \frac{W_t - W_0}{W_0} \times 100\%$$

where W_0 is the weight of the dry separator before swelling, and W_t is the weight of the separators swelling for a certain time t. Before measuring W_t, the swelled separators were wiped with filter paper to remove the extra liquid electrolyte on the surfaces.

A scanning electron microscope (Zeiss Merlin HRSEM) was used to examine the morphology of the rubber separators before and after swelling.

Tensile strength and elasticity tests were carried out using a Q800 Dynamic Mechanical Analyzer (TA instrument). The rubber and PP separator samples used are strips with a width of ~1.5 mm and length of ~2 cm, and the force loading and unloading rates were 0.5 N min^{-1}.

Discharge–charge cycles of the capillary cells were conducted using the Reference 3000 instrument. While cycling, the electrode section was videotaped by using an optical micro zoom inspection system (Scienscope, MZ7A).

Author contributions

K. L., C.-A. W. and J. L. conceived the research and designed the experiments. K. L. and P. B. designed the capillary cells, carried out the tests and analyzed the data. K. L. and P. B. wrote the paper, and all the authors contributed to revising the paper.

Acknowledgements

The authors acknowledge the support by NSF ECCS-1610806, and the grants from the National Natural Science Foundation of China (NSFC-No. 51572145 and 51221291).

References

1 P. G. Bruce, S. A. Freunberger, L. J. Hardwick and J. M. Tarascon, *Nat. Mater.*, 2012, **11**, 19.
2 W. Xu, J. Wang, F. Ding, X. Chen, E. Nasybulin, Y. Zhang and J. G. Zhang, *Energy Environ. Sci.*, 2014, **7**, 513.
3 D. Aurbach, E. Zinigrad, Y. Cohen and H. Teller, *Solid State Ionics*, 2002, **148**, 405.
4 D. Lu, Y. Shao, T. Lozano, W. D. Bennett, G. L. Graff, B. Polzin, J. Zhang, M. H. Engelhard, N. T. Saenz, W. A. Henderson, P. Bhattacharya, J. Liu and J. Xiao, *Adv. Energy Mater.*, 2015, **5**, 1400993.
5 P. Bai, J. Li, F. R. Brushett and M. Z. Bazant, *Energy Environ. Sci.*, 2016, **9**, 3221.
6 G. Bieker, M. Winter and P. Bieker, *Phys. Chem. Chem. Phys.*, 2015, **17**, 8670.
7 D. Aurbach, *J. Power Sources*, 2000, **89**, 206.
8 A. Kushima, K. P. So, C. Su, P. Bai, N. Kuriyama, T. Maebashi, Y. Fujiwara, M. Z. Bazant and J. Li, *Nano Energy*, 2017, **32**, 271.
9 A. Aryanfar, D. J. Brooks, A. J. Colussi and M. R. Hoffmann, *Phys. Chem. Chem. Phys.*, 2014, **16**, 24965.
10 R. Murugan, V. Thangadurai and W. Weppner, *Angew. Chem., Int. Ed.*, 2007, **46**, 7778.
11 H. Kitaura and H. Zhou, *Energy Environ. Sci.*, 2012, **5**, 9077.
12 H. Xie, Y. T. Li and J. B. Goodenough, *RSC Adv.*, 2011, **1**, 1728.
13 K. Liu and C. A. Wang, *Electrochem. Commun.*, 2014, **48**, 147.
14 M. Nakayama, S. Wada, S. Kurokic and M. Nogami, *Energy Environ. Sci.*, 2010, **3**, 1995.
15 R. Bouchet, S. Maria, R. Meziane, A. Aboulaich, L. Lienafa, J. P. Bonnet, T. N. T. Phan, D. Bertin, D. Gigmes, D. Devaux, R. Denoyel and M. Armand, *Nat. Mater.*, 2013, **12**, 452.
16 D. Zhang, R. S. Li, T. Huang and A. S. Yu, *J. Power Sources*, 2010, **195**, 1202.
17 Y. T. Chen, Y. C. Chuang, J. H. Su, H. C. Yu and Y. W. Chen-Yang, *J. Power Sources*, 2011, **196**, 2802.
18 J. H. Choi, C. H. Lee, J. H. Yu, C. H. Doh and S. M. Lee, *J. Power Sources*, 2015, **274**, 458.
19 B. Scrosati and J. Garche, *J. Power Sources*, 2010, **195**, 2419.
20 H. Wu, D. Zhuo, D. S. Kong and Y. Cui, *Nat. Commun.*, 2014, **5**, 5193.
21 C. Monroe and J. Newman, *J. Electrochem. Soc.*, 2005, **152**, A396.
22 N. Agmon, *Chem. Phys. Lett.*, 1995, **244**, 456.
23 M. Cappadonia, J. W. Erning, S. M. S Niaki and U. Stimming, *Solid State Ionics*, 1995, **77**, 65.
24 J. H. Han, E. Khoo, P. Bai and M. Z. Bazant, *Sci. Rep.*, 2014, **4**, 7056.
25 J. H. Han, M. Wang, P. Bai, F. R. Brushett and M. Z. Bazant, *Sci. Rep.*, 2016, **6**, 28054.
26 J. N. Chazalviel, *Phys. Rev. A: At., Mol., Opt. Phys.*, 1990, **42**, 7355.
27 M. Rosso, *Electrochim. Acta*, 2007, **53**, 250.
28 H. Fan, C. Hartshorn, T. Buchheit, D. Tallant, R. Assink, R. Simpson, D. J. Kissel, D. J. Lacks, S. Torquato and C. J. Brinker, *Nat. Mater.*, 2007, **6**, 418.
29 P. Cordier, F. Tournilhac, C. Soulie-Ziakovic and L. Leibler, *Nature*, 2008, **451**, 977.

Supporting information for

Soft non-porous separator and its effectiveness in stabilizing Li metal anode cycling at 10 mA/cm^2 observed in-situ in a capillary cell

Kai Liu,[1,2] Peng Bai,[3] Martin Z. Bazant,[3, 4] Chang-An Wang,[1, *] Ju Li[2,5,*]

[1] State Key Lab of New Ceramics and Fine Processing, School of Materials Science and Engineering, Tsinghua University, Beijing 100084, P. R. China.

[2] Department of Nuclear Science and Engineering, Massachusetts Institute of Technology, Cambridge, Massachusetts 02139, USA.

[3] Department of Chemical Engineering, Massachusetts Institute of Technology, Cambridge, Massachusetts 02139, USA.

[4] Department of Mathematics, Massachusetts Institute of Technology, Cambridge, Massachusetts 02139, USA.

[5] Department of Materials Science and Engineering, Massachusetts Institute of Technology, Cambridge, Massachusetts 02139, USA.

* Correspondence to: wangca@mail.tsinghua.edu.cn (C. Wang) or liju@mit.edu (J. Li)

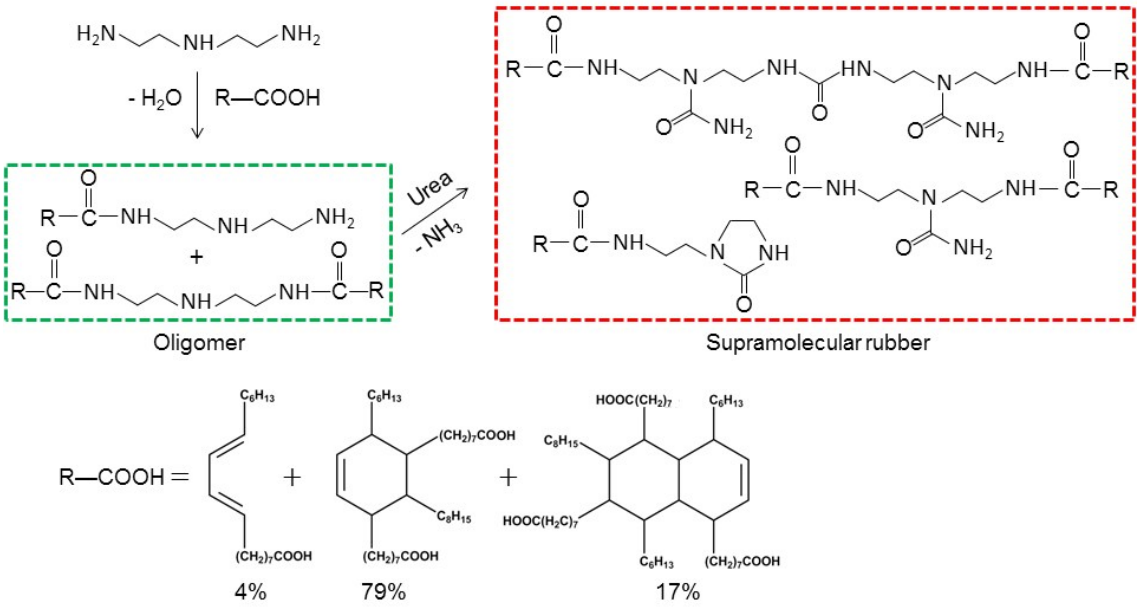

Fig. S1 Synthesis pathway and the molecule structures.

It should be mentioned that reaction of only one –COOH group in fatty dimmer acid R-COOH is showed, however, there are two or three –COOH groups in most of R-COOH molecules, and all of them can react with DETA resulting in cross-linked supramolecules.

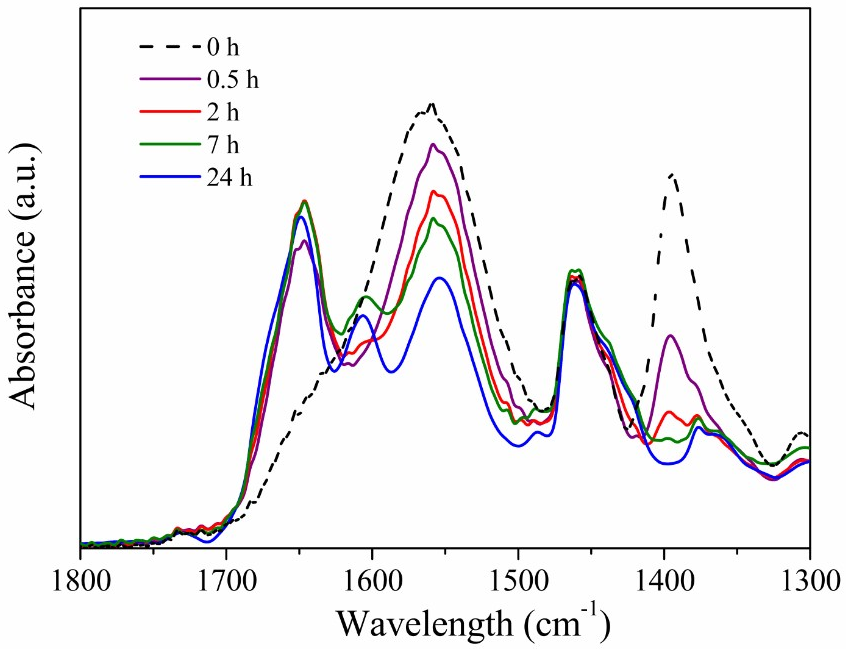

Fig. S2 FTIR spectra of the synthesis oligomer after 0 h, 0.5 h, 2 h, 7 h and 24 h of reaction. (Instrument: Vertex70v, Bruker)

While reaction time increases, the υs_{COO^-} and δ_{NH} signals at 1394 and 1550 cm^{-1} decreases, and the υ_{CO} amide signal at 1645 cm^{-1} appears right after the reaction begins. This result is well consistent with the result reported in reference [L. Leibler et al, Journal of Polymer Science: Part A: Polymer Chemistry, 2008, 46, 7925-7936], which confirm the reaction between –COOH groups in fatty dimmer acid and $–NH_2$ groups in DETA.

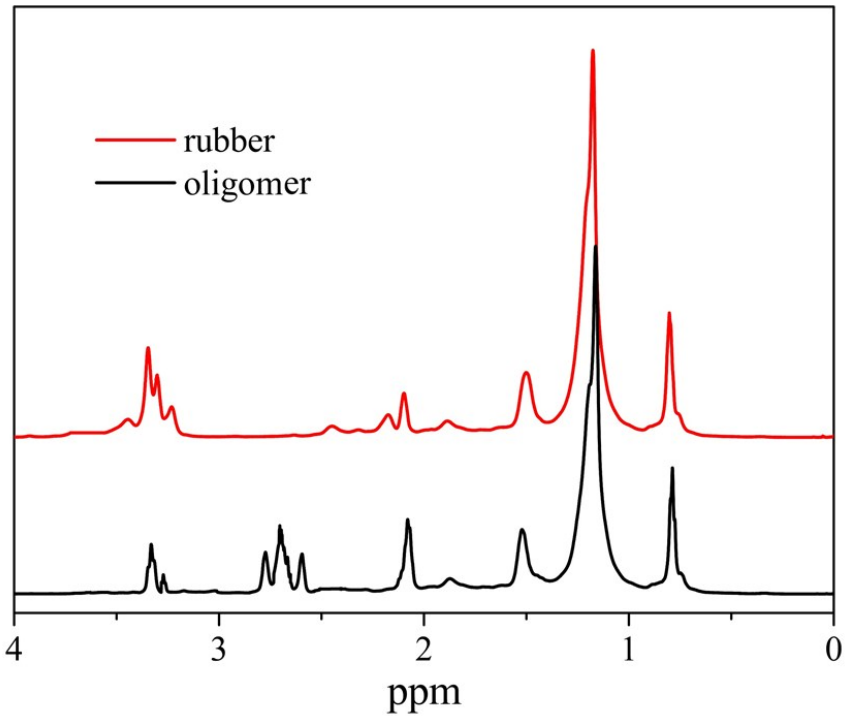

Fig. S3 NMR of the oligomer and the rubber. (Instrument: Varian Mercury 400 NMR spectrometer)

The peaks at 2.6 and 2.8 corresponds to the protons on CH_2 connected to primary amines. The peaks at 2.7 corresponds to the protons on -CH_2 groups connected to secondary amines. Upon reaction, as can be seen in the spectra of the rubber, all the three peeks disappeared, indicating that the primary amine groups and secondary amine groups were converted into urea. This result is also consistent with the results in references [L. Leibler et al, Journal of Polymer Science: Part A: Polymer Chemistry, 2008, 46, 7925-7936] and [Z. Bao et al, Nature Chemistry, 2013, 5, 1042-1048].

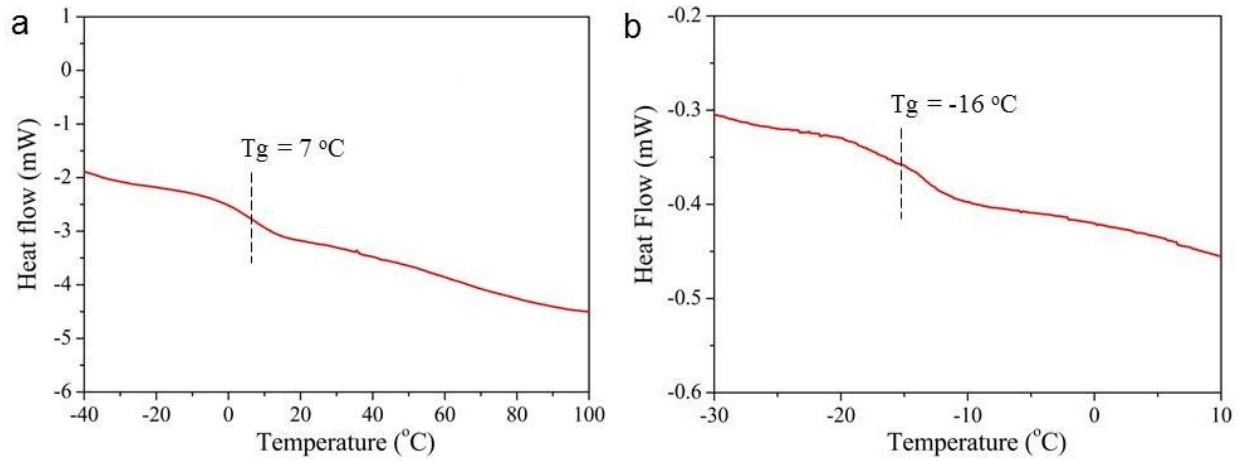

Fig. S4 Differential scanning calorimetry (DSC) traces of the rubber separator before swelling (a) and after swelling (b). The experiment was conducted at a heating rate of 10 °C/min under N_2 atmosphere. (Instrument: DSC Q2000, TA Instruments)

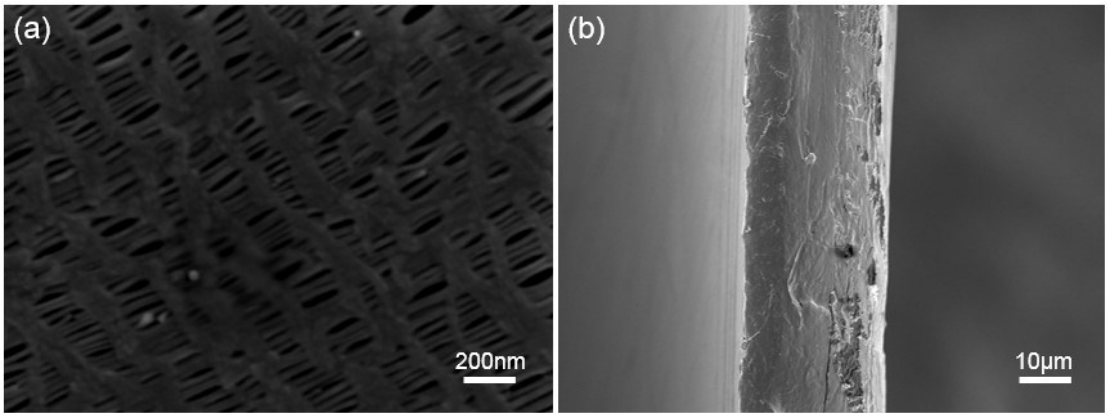

Fig. S5 SEM images of the commercial porous PP separator (Celgard 2400). (a) Surface, top view; (b) cross section, side view.

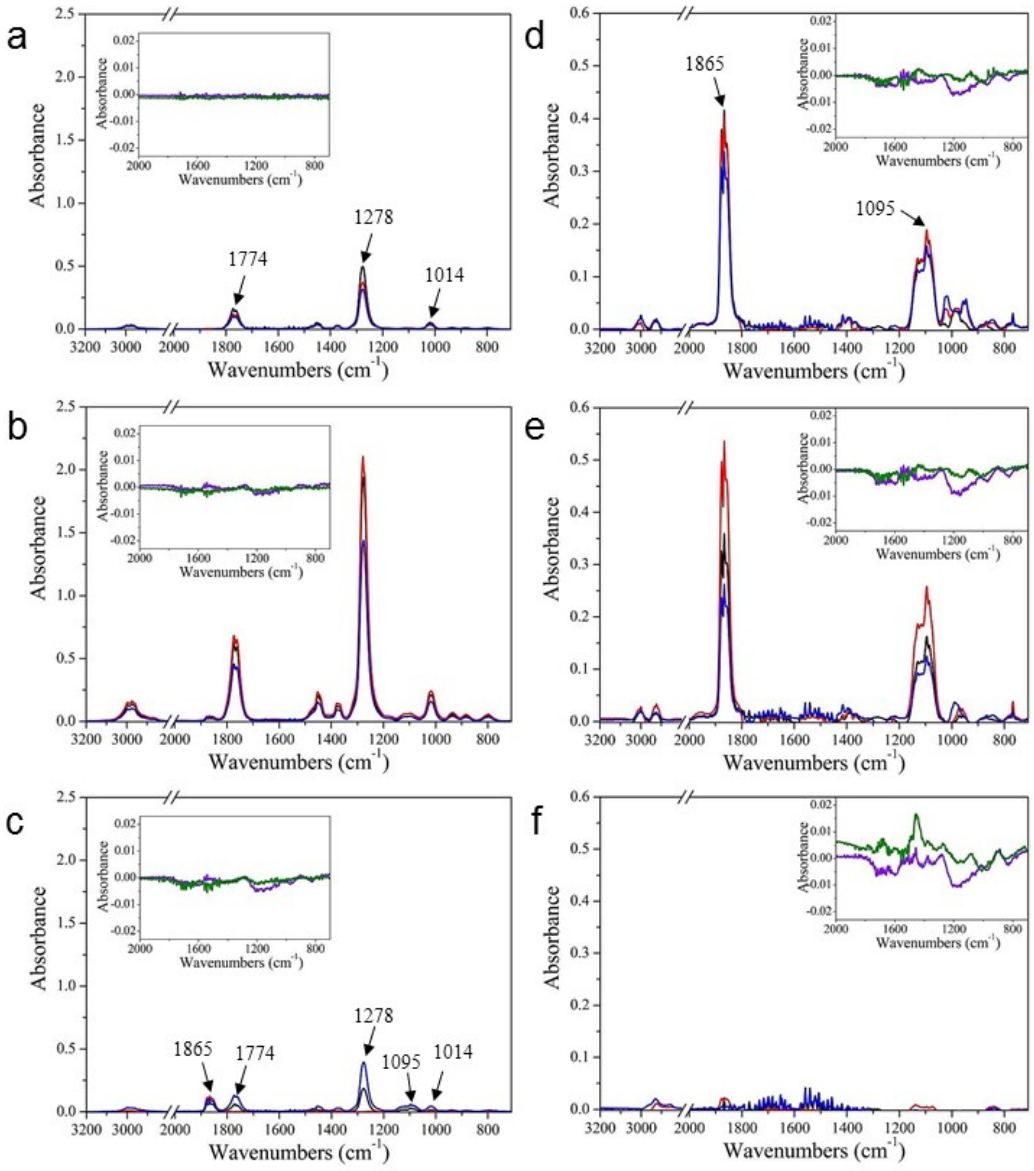

Fig. S6 FTIR Spectra of the vapor come out from the samples at different temperatures. (a) 50 °C; (b) 100 °C; (c) 150 °C; (d) 220 °C; (e) 300 °C; (f) 450 °C. For all the images, black line: 1 M $LiPF_6$ in EC/MEC (3:7 by volume) liquid electrolyte; red line: the liquid electrolyte swelled celgard 2400; blue line: the liquid electrolyte swelled rubber separator; insert purple line: dry (pristine) celgard 2400; insert green line: dry (pristine) rubber membrane. (Instrument: Vertex70v, Bruker)

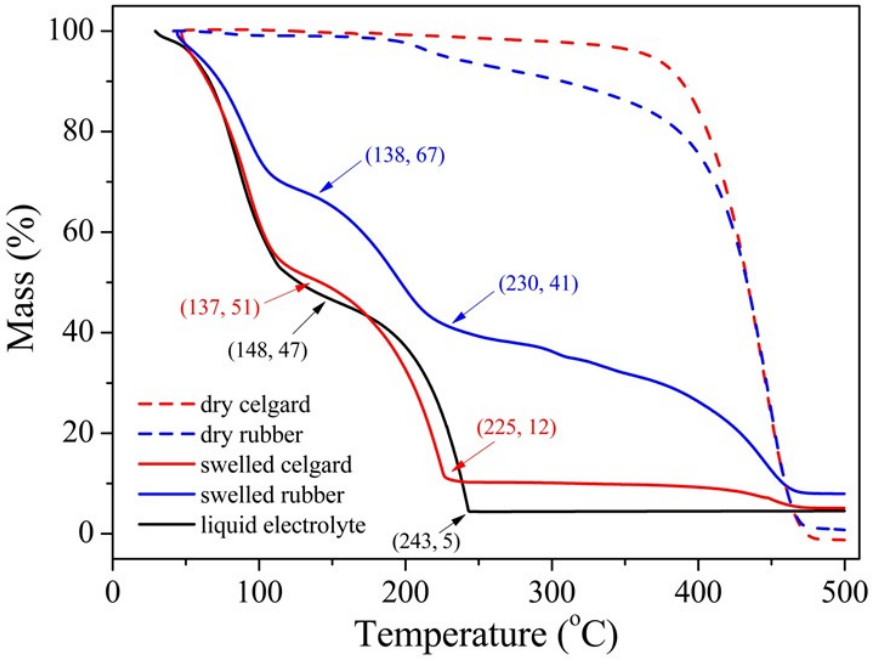

Fig. S7 Thermogravimetric curves of the 1 M $LiPF_6$ in EC/MEC (3:7 by volume) liquid electrolyte and separators. Temperature range: room temperature to 500 °C; heating rate: 5 °C/min; atmosphere: Ar. (Instrument: QMS 403C, Netzsch)

The thermogravimetric curve of the liquid electrolyte can be divided into three sections: section 1) room temperature to 148 °C, in which the whole mass loss is 53%; section 2) 148 °C to 243 °C, and the mass loss is 42%; section 3) 243 °C to 500 °C, no mass loss. According to the composition of the liquid electrolyte and the densities of the components, we can calculate that the mass percentage of the EMC, which has much lower boiling point than EC and should evaporate first, is ~55%, very close to the mass loss in section 1. From Figure S6 we can see, at 50 °C and 100 °C, the peeks of the liquid electrolyte's spectra are well consistent with the peeks of chain carbonate [http://webbook.nist.gov/cgi/cbook.cgi?ID=C616386&Units=SI&Type=IR-SPEC&Index=1#IR-SPEC; http://webbook.nist.gov/cgi/cbook.cgi?ID=C105588&Units=SI&Type=IR-SPEC&Index=1#IR-SPEC], so we can conclude that in section 1, the main vapor came out is EMC. In section 2, the vapor's FTIR peeks (Figure S6(d)) can be well identified as EC [http://webbook.nist.gov/cgi/cbook.cgi?ID=C96491&Units=SI&Type=IR-SPEC&Index=0#IR-SPEC]. However, the mass loss in section 2 (42%) is higher than the mass percentage of EC in the liquid

electrolyte (32%). The mass loss different could come from the loss of PF_5 gas generated from the decomposition of $LiPF_6$. The ratio between the mass loss in section 1 and section 2 is 53/42=1.26. In section 3, there was no mass loss, but FTIR signals could still be observed, which may due to the evaporation of EC condensed inside the connecting tubes (kept at 200 ^oC during the whole test) of the instruments. The final mass remained in section 3 (5%) should be generally positively related to to the mass percentage of $LiPF_6$ salt. In summary, these TG-FTIR results can roughly and effectively confirm the composition of the liquid electrolyte.

Based on the analysis of the liquid electrolyte TG-FTIR results, the behaviour of Celgard 2400 and the rubber samples under heating can be well understood. For the swelled Celgard separator, its TG curve can also be divided into the same 3 sections (demarcation points are 137 and 225 ^oC). The ratio between the mass loss in section 1 and section 2 is 49/39=1.26, the same as the results of the liquid electrolyte sample. The FTIR signals at different temperatures are also highly similar to liquid eletrolyte's signals. For the swelled rubber separator, the demarcation points of its TG curve are 138 and 230 ^oC, and the ratio between the mass loss in section 1 and section 2 is 33/26=1.27, and the FTIR signals are highly similar as well. These results indicate that the liquid electrolytes imbibed into both two kind of separators have solvents with the same composition as the bulk liquid electrolyte's solvent.

The difference of the final masses remained at 500 ^oC between swelled and dry samples are positively relevant to the mass percentage of $LiPF_6$ salt uptook into the separator. For Celgard and the rubber samples, the differences are 6% and 7% respectively. Considering the mass percentage of liquid electrolyte imbibed (~90% and ~60% for Celgard and rubber, respectively), it seems that the liquid electrolyte imbibed into the rubber separator has a much higher $LiPF_6$ salt concentration, but further investigation is needed to confirm.

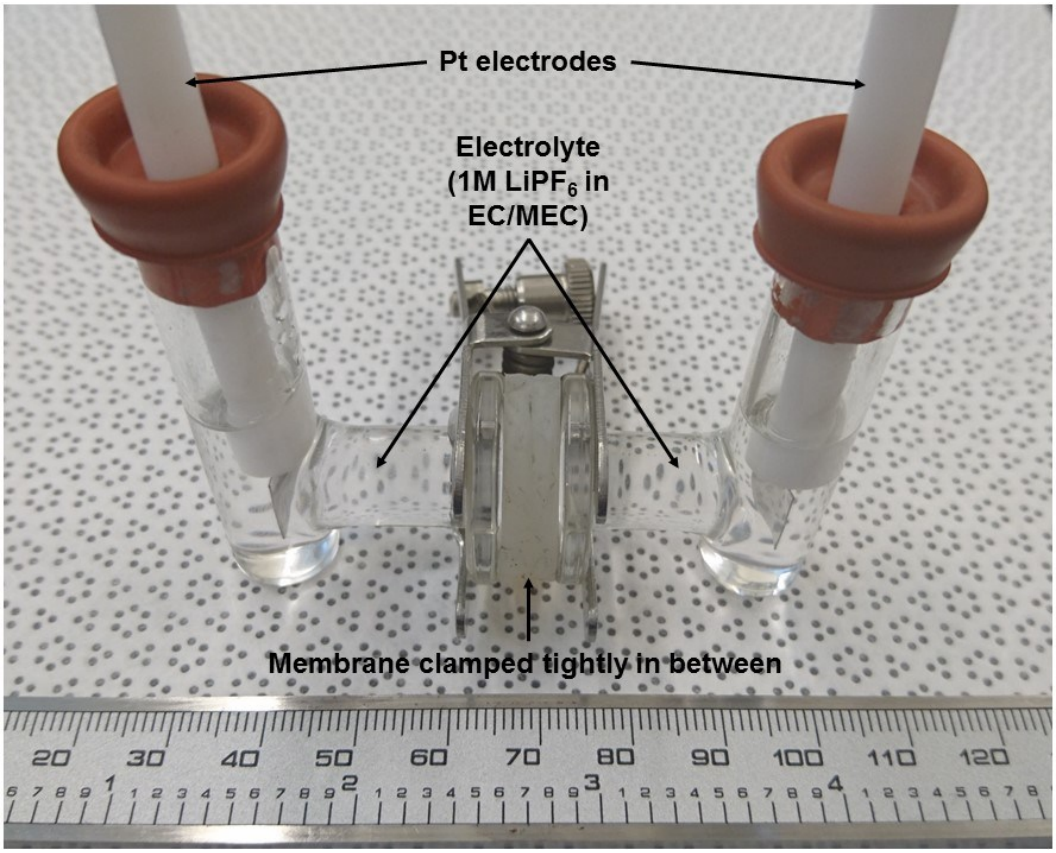

Fig. S8 Photo of an H-type cell

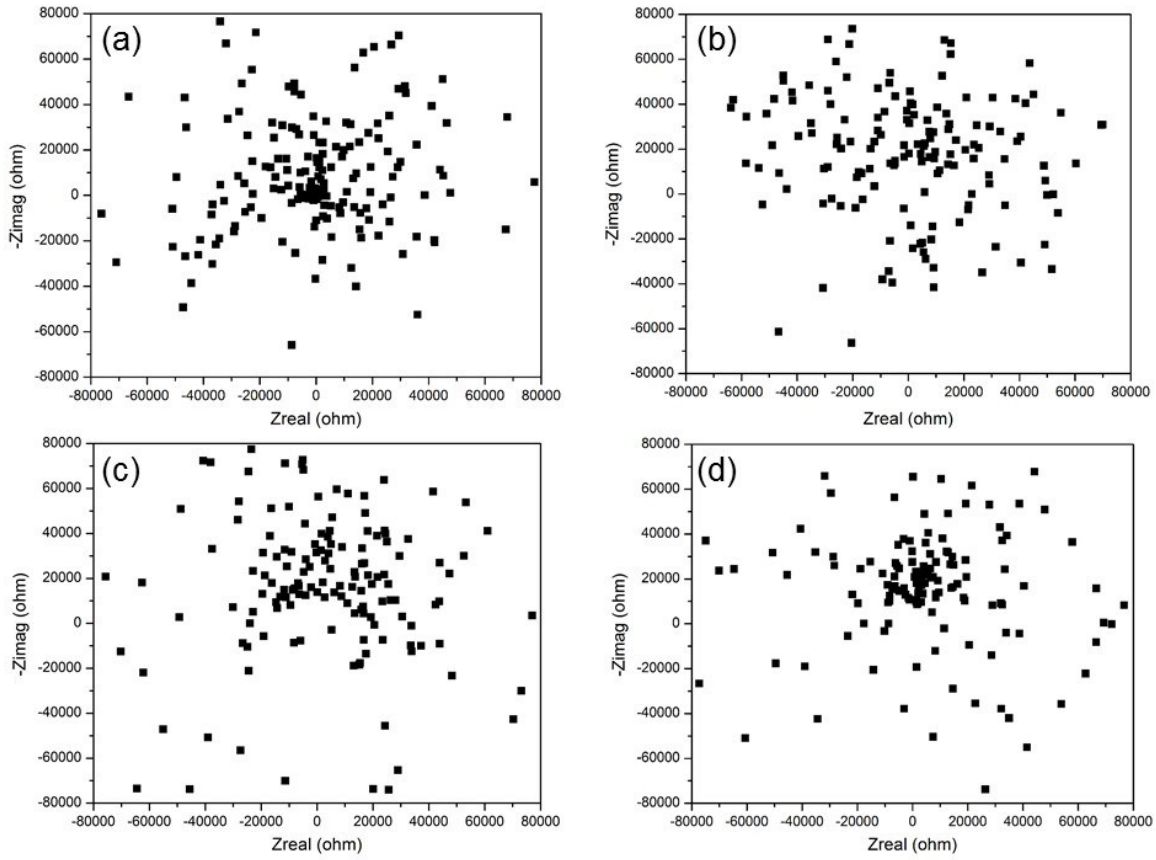

Fig. S9 AC impedance spectrum of the H-type cell with (a) dense PVDF separator with no lithium ionic conductivity and the non-porous rubber separator after soaking for (b) 0 h, (c) 0.5 h and (c) 1 h.

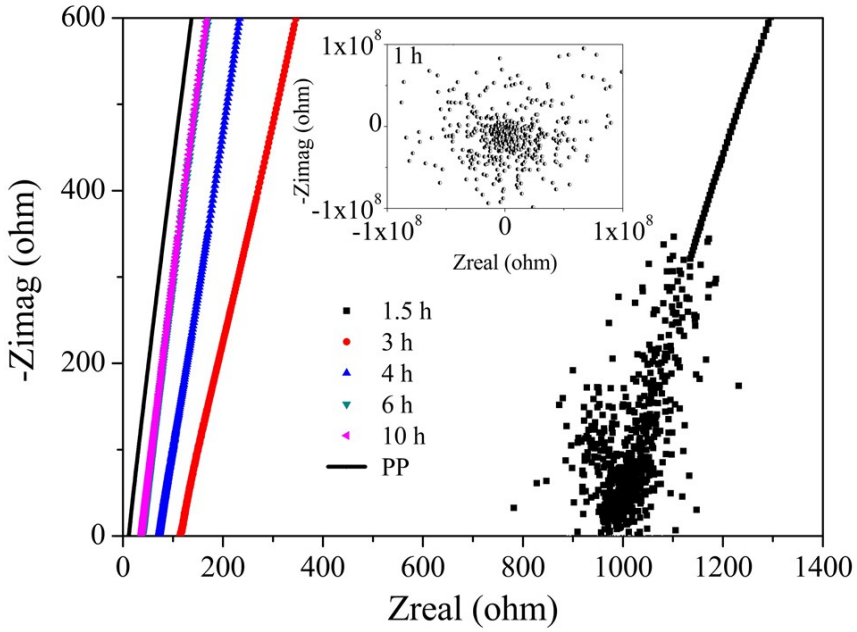

Fig. S10 AC impedance spectra of sandwich structured stainless steel/separator/staniless steel cells with wetted PP separator and rubber separators swelled for 1 h~10 h.

The impedance spectra change of the rubber separator swelled with soaking time showed the same trend as the results of H-type cell.

The whole cell resistance of the rubber separator based cell (38 Ω) is ~3 times bigger than that of the PP separator based cell (11 Ω). Considering the rubber separator is ~2 time thicker than the PP separator, their ionic conductivities in coin cells are at the same level.

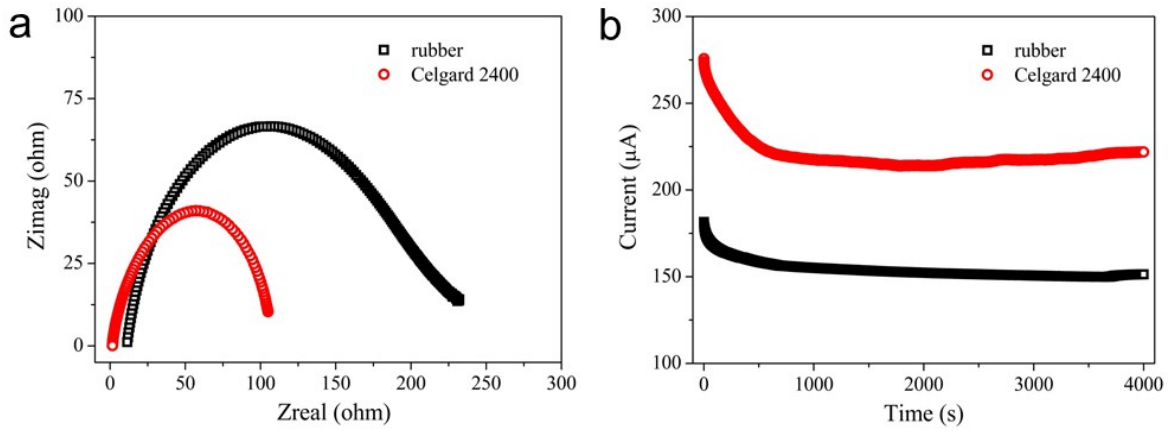

Fig. S11 The lithium-ion transference numbers test. (a) AC impedance spectroscopy (40~110 MHz) of coin cells employing Celgard 2400 and the rubber separator, respectively. Cells are tested 1 day after assembling. (b) DC polarization curves of the cells. V_{DC}=50 mV.

We tested the t+ using the method reported by L. Suo et al [L. Suo et al, Nature Communications, 2013, 4:1481, DOI: 10.1038/ncomms2513]. The Li ion transference number can be calculated as: $t_+=I_{Dc}\times R_{cell}/V_{DC}$, where V_{DC} is the voltage used in DC polarization, I_{DC} is the stable current obtained, and R_{cell} is total resistance of the cell obtained from AC impedance test. For celgard 2400: I_{DC}=220 μA, R_{cell}=108 Ω; for the rubber separator: I_{DC}=151 μA, R_{cell}=252 Ω. Then we can get the Li ion transference numbers: $t_{+\ Celgard}$=0.48 and $t_{+\ rubber}$=0.76. As can be seen, the Li ion transference number of the rubber separator is much higher than that of the celgard 2400 separator.

We assume that in the porous celgard 2400, the separator matrix has little chemical interaction with the uptaken liquid organic electrolyte, so the liquid electrolyte inside the pores has the same properties as bulk liquid electrolyte, including Li^+ transference number, which is known to be quite low, as a consequence, the wetted celgard separator inside the cell showed a low t_+. However, in the rubber separator, the rubber molecule has weakly acidic protons, which would form hydrogen bonds with F atoms in $[PF_6]^-$, so that to some extent confine the movement of the anions and resulting in a higher t_+.

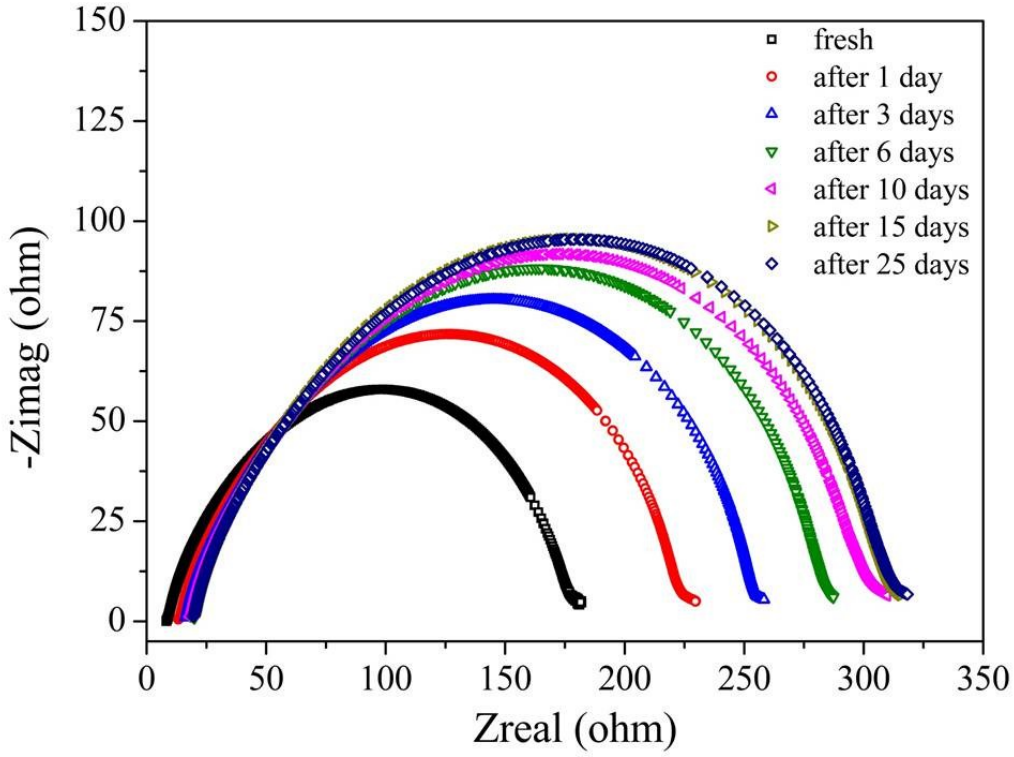

Fig. S12 Impedance spectra of Li/rubber separator/Li cell

The cell resistance increased with time and leveled off at ~320 Ω after 25 days, which indicates the existance of side reactions between lithium metal and the rubber separator on their interface. However, the resistance and the increase of the resistance are not too large and would not affect the application of the rubber separator seriously.

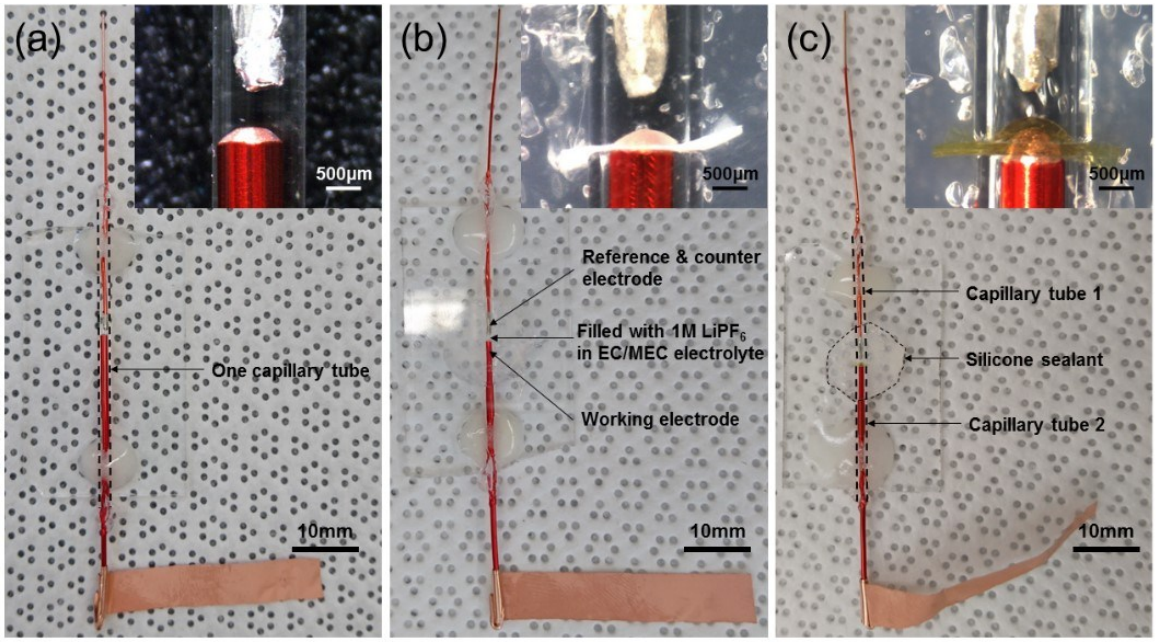

Fig. S13 Structure of capillary cells with (a) no separator, (b) the porous PP separator and (c) the rubber separator between two electrodes. The insert in each picture is an enlarged view of the electrodes section.

For the cells using a separator, two short capillary tubes were joined together head-to-head with the separator clamped and fixed in between, and the connection was sealed with clear silicone sealant. For the cell without a separator, only one long capillary tube was used. All the capillary cells were fixed on a piece of glass plate. Electrodes and electrolytes were loaded inside a glovebox filled with argon gas. In each cell, a piece of lithium metal was wrapped around an exposed end of a thin enameled copper wire and acted as counter and reference electrodes. A thick enameled copper wire with a round exposed head was used as working electrode. After injection of liquid electrolyte, the open ends of the capillary tubes were sealed and the cells were taken out of glovebox.

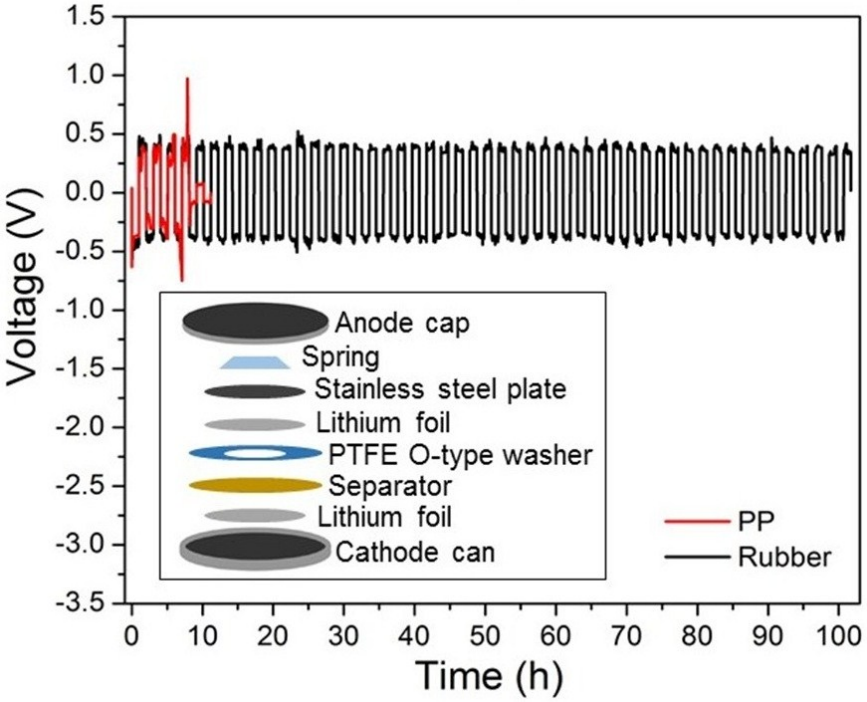

Fig. S14 Cycling profile of Li-Li symmetrical cells at a current density of 10 mA cm^{-2}, and areal capacity of 10 mAh cm^{-2}. Insert is the structure of the symmetrical cell. Note that a 50-μm-thick PTFE washer was sandwiched between anode and the separator to fix the position of the separator and reserve space for the lithium anode volume change.

For the cell with porous PP separator, after only 4 cycles, the voltage dropped dramatically, as a result of internal short due to lithium dendrite penetration. In contrast, the cell with our rubber separator was cycled for 50 cycles, and no internal short was observed. Although the Young's modulus of the soft, swollen rubber separator are lower than the 6.8 GPa limit by a factor of 10^4-10^5, it can still prevent the lithium dendrite penetration and survive in large electrode volume change at a high current density of 10 mA cm^{-2} and a high capacity of 10 mAh cm^{-2} for very long time.

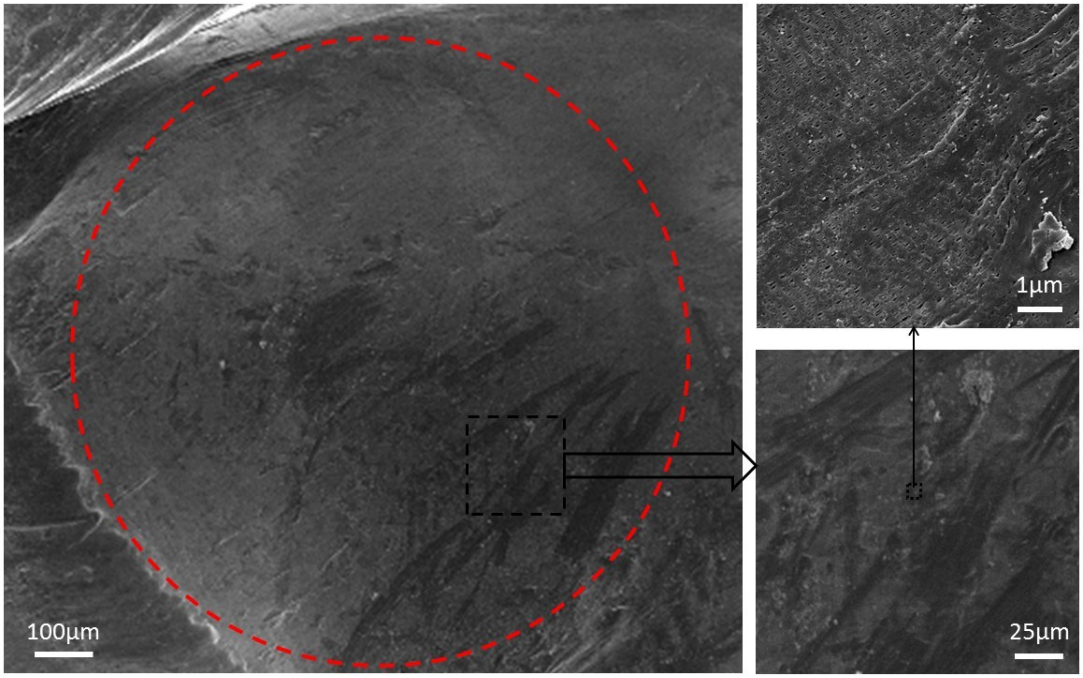

Fig. S15 SEM images of the PP separator after used in the capillary cell.